An Efficient Technique for Designing High-Performance Millimeter-Wave Vector Modulators With Low Temperature Drift

Yang Hou, *Student Member, IEEE*, Lingyun Li, Rong Qian, and Xiaowei Sun, *Member, IEEE*

***Abstract*—Recently the demand for high-performance low-cost vector modulators for millimeter-wave direct carrier modulation applications is increasing. An efficient technique to improve the performance of the vector modulators has been proposed in this paper accordingly. This technique highlights the effect of the Lange coupler characteristic impedance and the cold pseudomorphic HEMT (pHEMT) total gatewidth on the performance. It is demonstrated by investigating two types of vector modulators, which employ unbalanced and balanced topologies. Furthermore, to reduce the temperature drift, a concise analysis of the thermal behavior of the vector modulators has been carried out. Based on the proposed technique, two types of monolithic vector modulators have been realized at 40 GHz on a 100-μm-thick GaAs substrate with 0.15-μm cold-pHEMT devices. The static constellations were obtained by using an automatic measurement system, and the temperature drifts were characterized by the measurement data from −55 °C to 70 °C. The results show that the technique is suitable for millimeter-wave vector modulator designs.**

***Index Terms*—HEMT, millimeter-wave circuits, monolithic microwave integrated circuits (MMICs), vector modulator.**

I. Introduction

SOPHISTICATED phase and amplitude modulation is one of the key techniques used in millimeter-wave high-speed access systems. Normally, it is achieved by a complex and costly up-converter chain, which consists of baseband modulator, mixers, filters, and amplifiers. The in-phase and quadrature-phase (I-Q) vector modulator is now innovated to reduce the front-end cost and complexity for its capability of direct carrier modulation, and it gradually plays a significant role in modern wireless communication systems [1], [2].

A general approach to realize a vector modulator in microwave and millimeter-wave application is based on two orthogonal bi-phase amplitude modulators connected with an in-phase coupler. These two bi-phase amplitude modulators are voltage controlled independently, and therefore, can simultaneously control the phase and amplitude of the output under the vector addition law. The bi-phase amplitude modulators primarily determine the performance of the vector modulators.

The first bi-phase amplitude modulator proposed and applied in monolithic microwave integrated circuit (MMIC) design utilized the reflection type topology [3]. A variable resistance reflection termination is used to control the attenuation level of the amplitude modulator. In GaAs MMICs, field-effect transistors (FETs) and HEMTs are generally selected as the variable resistance elements. However, the parasitics will deteriorate the constellation symmetry at millimeter-wave frequencies, which makes the vector modulator difficult to use. To remove the imbalance of the constellation, the balanced, or push–pull, bi-phase amplitude modulator has been innovated [4], [5]. Besides constellation symmetry, the minimum insertion loss is a significant quality of the vector modulator. This value varies with different design methods and fabrications. Reducing the minimum insertion loss can increase the constellation size and the distance of neighbor modulation code words, and therefore, it can decrease the error probability in communication. Temperature drift is also a critical character of the vector modulators. Many applications in adverse circumstance may request the vector modulator less sensitive to the ambient temperature.

In this paper, a technique to realize high-performance and low-temperature drift vector modulators is presented. First, to detail the principles and behavior of the vector modulator, Section II characterizes the cold pseudomorphic HEMT (pHEMT) terminations and investigates the practical performance of two different bi-phase amplitude modulators. Section II illustrates how to effectively improve the amplitude modulators by adjusting the parameters of cold-pHEMT and Lange couplers. Section III uses a first-order approximated model to analyze the temperature behavior of the vector modulator, and gets a simple and clear method to improve the temperature performance. However, the way to reduce the temperature drift is in conflict with that to improve the modulating performance. Thus, Section IV makes a compromise between the two design targets, and finally summaries the circuit design procedures and measurement results.

II. Analysis of the Circuit

To implement an I-Q vector modulator, the basic schematic diagrams and principles are shown in Fig. 1. The 3-dB Lange coupler splits the input signal into two orthogonal portions: in-phase and quadrature-phase. These two portions are attenuated by two bi-phase amplitude modulators, which are controlled by two bias voltages V_I and V_Q. Combining these

Manuscript received April 23, 2008; revised July 07, 2008. First published November 18, 2008; current version published December 05, 2008.

The authors are with the Shanghai Institute of Microsystem and Information Technology, Chinese Academy of Science, Shanghai 200050, China, and also with the Graduate University of Chinese Academy of Sciences, Beijing 100049, China (e-mail: houyang@mail.sim.ac.cn; lilingyun@mail.sim.ac.cn; qrong@mail.sim.ac.cn; xwsun@mail.sim.ac.cn).

Digital Object Identifier 10.1109/TMTT.2008.2006808

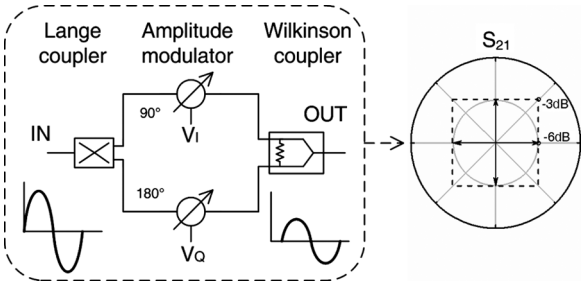

Fig. 1. Schematic diagrams and basic principles of the vector modulator.

two modulated portions with a Wilkinson coupler completes the modulating function.

Assume that the input is an amplitude normalized signal with the frequency of ω, the voltage of output $v(t)$ can be written as

$$v(t) = \frac{1}{\sqrt{2}} \times \frac{1}{\sqrt{2}} \left(S_{I21} + jS_{Q21}\right) e^{j(\omega t+\varphi)} \tag{1}$$

where the constant coefficient $1/\sqrt{2}$ is induced by the 3-dB coupler; S_{I21}, S_{Q21} are the transmission coefficients of the bi-phase amplitude modulators, respectively, and φ is the additional constant phase shift. The insertion loss $\mathbb{IL}$ and phase shift θ of the vector modulator can be obtained as follows:

$$\mathbb{IL} = -6 + 20\log\left|\sqrt{|S_{I21}|^2 + |S_{Q21}|^2}\right| \tag{2}$$

$$\theta = \varphi + \tan^{-1}\frac{S_{Q21}}{S_{I21}}. \tag{3}$$

Theoretically, both S_{I21} and S_{Q21} are between -1 and 1 if the bi-phase amplitude modulators are passive. As Fig. 1 shows, the vector modulator has an inherent 3-dB minimum insertion loss and a 6-dB omnidirectional insertion loss. Further investigation on vector modulators essentially requires characterizing the variable resistance terminations and precisely analyzing the bi-phase amplitude modulators.

A. Scalable Cold-pHEMT Model

Variable resistance terminations are the key devices in most electric control circuits such as switchers, phase shifters, and amplitude attenuators. Current-controlled p-i-n diodes are conventionally used to realize a variable resistor with hybrid integrated technology. Since the p-i-n diode needs significant control power and its foundry processing is not easily compatible with others, a voltage-controlled FET is, therefore, selected as a variable resistor with MMIC technology. High electron-mobility transistors including pHEMTs and metamorphic HEMTs (mHEMTs) are also available in MMIC technology when the circuit operating frequency increases up to the millimeter-wave band. Here, in this application, a standard common-source pHEMT with zero bias voltage applied to the drain is employed.

Fig. 2(a) shows the one-port small-signal model of the cold-pHEMT. Only three elements, i.e., $C_{\rm gs}$, $C_{\rm gd}$, and $R_{\rm ds}$ are bias dependent. The gate contact resistance R_g and inductance L_g

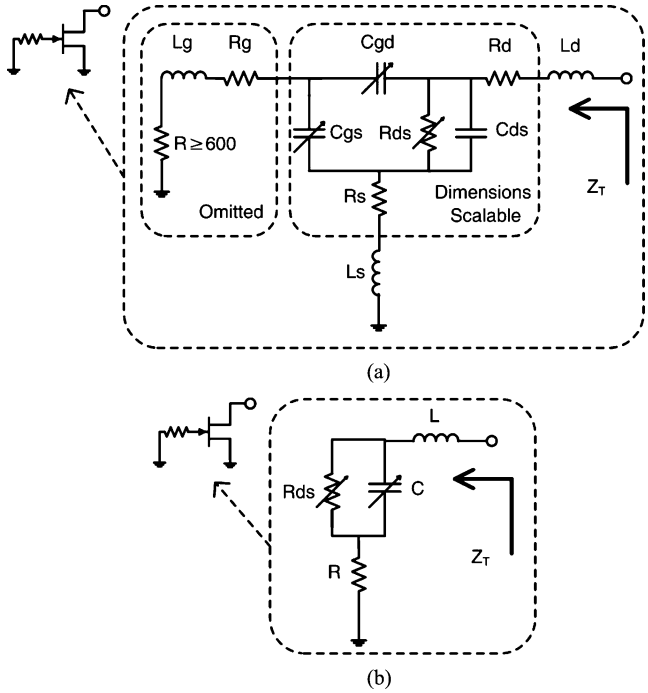

Fig. 2. Circuit diagrams of: (a) small-signal model of a cold-pHEMT and (b) simplified equivalent circuit of a cold-pHEMT.

have little effect on terminal impedance Z_T since they are absorbed by a large gate biasing resistor, which makes the gate as open [6]. Let

$$C = \frac{C_{\rm gs}C_{\rm gd}}{C_{\rm gs}+C_{\rm gd}} + C_{\rm ds} \tag{4}$$

$$R = R_d + R_s \tag{5}$$

$$L = L_d + L_s. \tag{6}$$

The one-port small-signal model of the cold-pHEMT can be simplified as shown in Fig. 2(b). This model is generally dimension scalable, the scaling factor F is defined by

$$F = \frac{W_t}{W_u} = \frac{W \times N}{W_u} \tag{7}$$

where W, W_t, W_u, and N are the gatewidth, total gatewidth, unit gatewidth, and number of fingers, respectively. The model parameters are scaled according to the following equations:

$$C = C_0 + C_u \times F \tag{8}$$

$$R_{\rm ds} = \frac{R_{{\rm ds}u}}{F} \tag{9}$$

and the suffix u indicates the device parameters of unit gatewidth device. According to the dimension scalable model, the characters of the cold-pHEMT with arbitrary gatewidth can be approximately estimated by characterizing several different size cold-pHEMTs.

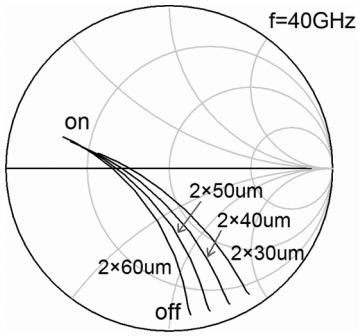

Fig. 3. Terminal impedance of different size cold-pHEMTs.

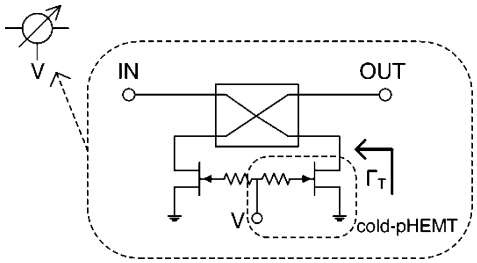

Fig. 4. Schematic of the unbalanced reflection-type bi-phase amplitude modulator.

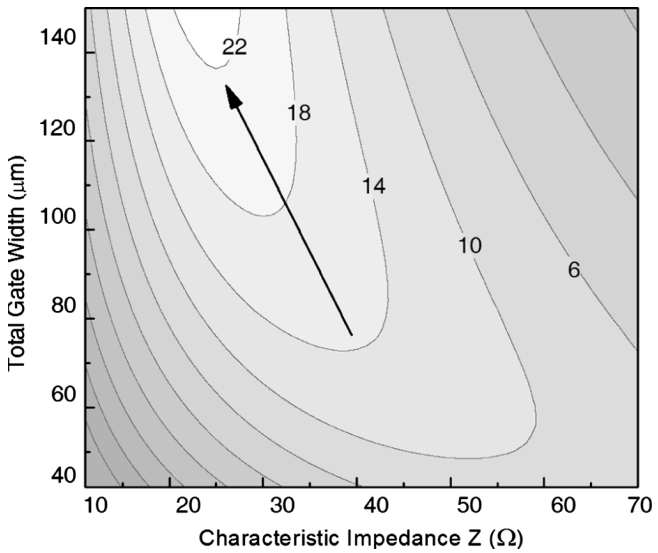

Fig. 5. Evaluation factor of the unbalanced bi-phase amplitude modulator.

An ideal cold-pHEMT has zero drain–source resistance at forward bias and infinite resistance when pinched off. In practice, the terminal impedance of the cold-pHEMT Z_T is given by

$$Z_T = R + j\omega L + \frac{R_{\rm ds}}{1 + j\omega R_{\rm ds} C}. \tag{10}$$

Although channel resistance $R_{\rm ds}$ varies from a few ohms up to several kiloohms as the bias voltage sweeps, the contact resistance R and inductance L cause the total impedance much more than zero at forward bias and the shunt capacitance C diminishes the large pinch-off resistance. Fig. 3 illustrates the terminal impedance of different cold-pHEMTs as the voltage bias sweeping from -1 to 0.5 V.

B. Unbalanced Bi-Phase Amplitude Modulator

The unbalanced bi-phase amplitude modulator is based on a reflection type topology, as shown in Fig. 4. This topology employs a 3-dB Lange coupler and a pair of cold-pHEMT terminations. The Lange coupler splits the input signal equally between direct and coupled ports with 90° phase shift. When two orthogonal portions are reflected back to the coupler, they are cancelled at the input port and reduplicated at the isolated port. As the resistance of the termination varies from low to high, signals are reflected with different attenuations. Conventional designs choose the characteristic impedance of the Lange coupler equal to 50 Ω, which makes the input and output ports perfectly matched. However, the impedance value has a significant effect on the performance of the amplitude modulator [7]. Assuming the impedance of the Lange coupler is Z and the port impedance is 50 Ω, the S-parameter matrix of the unbalanced bi-phase amplitude modulator is given by

$$[S] = \begin{bmatrix} \Gamma_T^2 \dfrac{Z-50}{Z+50} & -j\Gamma_T \\ -j\Gamma_T & \Gamma_T^2 \dfrac{Z-50}{Z+50} \end{bmatrix} \tag{11}$$

where Γ_T is the reflection coefficient of the cold-pHEMT termination given by

$$\Gamma_T = \frac{Z_T - Z}{Z_T + Z}. \tag{12}$$

The maximum magnitude of the transmission coefficient can be achieved when the cold-pHEMT is in the on-state or off-state. For an ideal bi-phase amplitude modulator, the maximum in-phase and antiphase transmission coefficients have the equal amplitude and a 180° phase shift. Actually, the asymmetry exists due to the parasitical elements of the cold-pHEMT terminations and the unbalanced circuit topology. The phase asymmetry $\Delta\theta$ and the amplitude asymmetry $\Delta\Gamma$ of the unbalanced amplitude modulator are defined by

$$\Delta\theta = \angle\Gamma_{\rm on} - \angle\Gamma_{\rm off} - 180^\circ \tag{13}$$

$$\Delta\Gamma = |\Gamma_{\rm on}| - |\Gamma_{\rm off}|. \tag{14}$$

In order to obtain the high-performance design, these two values of asymmetries should be diminished. This paper proposed an evaluation factor ef_U to reveal both the angle and amplitude asymmetries, and it is defined as

$$\mathrm{ef}_U = 20\log\left|\frac{\Gamma_{\rm on} - \Gamma_{\rm off}}{\Gamma_{\rm on} + \Gamma_{\rm off}}\right|. \tag{15}$$

This evaluation factor can be used to estimate the performance of the circuit designs, and as the value of the factor increases, the circuit performs better. For an ideal bi-phase amplitude modulator, the value will be $+\infty$. Fig. 5 contours the value of the evaluation factor with the total gatewidth ranging between 40–150 μm, and the characteristic impedance Z ranging between 10–70 Ω. Obviously as the arrow points, the evaluation factor increases when parameters tend toward 150 μm and 25 Ω. The arrow crosses the region, which has lower gradient value, and the circuit designed in this region, will be less sensitive to the fabrication spread [8].

C. Balanced Bi-Phase Amplitude Modulator

The balanced bi-phase amplitude modulator, which employs two reflection type bi-phase amplitude modulators operated

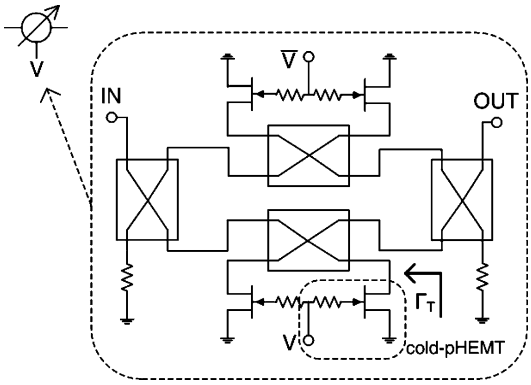

Fig. 6. Schematic of the balanced push–pull bi-phase amplitude modulator.

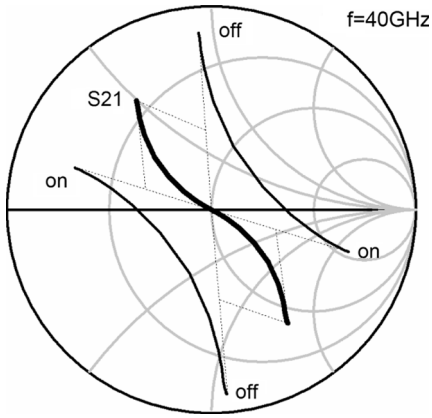

Fig. 7. Simulated S_{21} of the balanced push–pull bi-phase amplitude modulator.

in push–pull mode, is introduced to cancel the amplitude and phase asymmetries caused by the parasitic elements of the cold-pHEMT. The circuit schematic of the balanced bi-phase amplitude modulator is shown in Fig. 6; two reflection type amplitude modulators are controlled by the complementary bias voltages and the two Lange couplers realize the image 180° shift.

The voltage transmission coefficient S_{21} of the balanced bi-phase amplitude modulator is given by

$$S_{21} = \frac{j}{2}\left[\Gamma_T(V) - \Gamma_T(\bar{V})\right] \tag{16}$$

where V is the bias voltage applied to the gate, and the two voltages have an experimental relationship as

$$\bar{V} = -0.75 - V. \tag{17}$$

Fig. 7 shows the simulated S_{21} of the bi-phase amplitude modulator with 2×60 μm cold-pHEMT terminations, as the bias voltage sweeping from -1 to 0.5 V. It can be seen the response is perfectly symmetrical with ideal Lange couplers. Unlike the unbalanced topology, the maximum transmission coefficient is used to evaluate the performance of the balanced bi-phase amplitude modulator. The maximum magnitude of the transmission coefficient can be reached when one unbalanced branch works at the on-state and the other branch works at off-state, and therefore, the evaluation factor ef_B is defined as

$$\mathrm{ef}_B = 20\log\left|\frac{\Gamma_{\mathrm{on}} - \Gamma_{\mathrm{off}}}{2}\right|. \tag{18}$$

As the magnitude of the reflection coefficient is always less than 1, the value of the factor is negative and the circuit performs better as the evaluation factor increases. For an ideal bi-phase amplitude modulator, the value will be zero. Fig. 8 illustrates the simulated contour lines of the evaluation factor, as the total gatewidth ranging between 40–150 μm, and the characteristic impedance Z ranging between 10–70 Ω. Obviously as the arrow points, the evaluation factor increases when total gatewidth increases and characteristic impedance tends towards 30 Ω. The arrow also crosses the region, which is less sensitive to the fabrication spread.

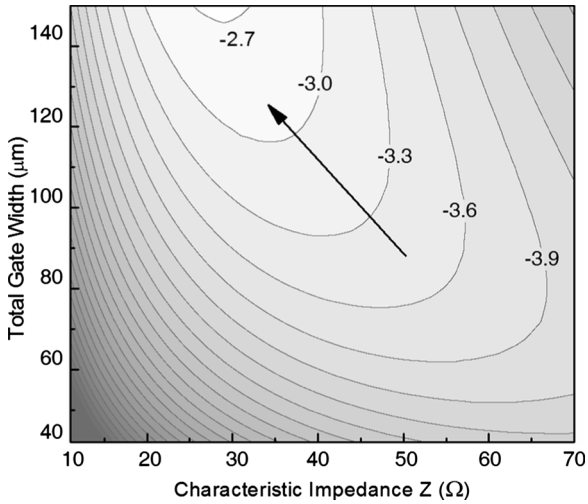

Fig. 8. Evaluation factor of the balanced bi-phase amplitude modulator.

III. Optimization of the Temperature Performance

Most electron devices are sensitive to the temperature, and the circuits with low temperature drift can fit a wide range of applications. The cold-pHEMT terminations are the main temperature-dependent devices inside the vector modulators. This paper uses the simplified equivalent model in Fig. 2(b) to analyze the temperature behavior of the cold-pHEMT. The temperature coefficient α of a parameter X is defined as the relative slope of the X temperature function [9]. The α is normalized to the temperature 20 °C at which S-parameters are measured

$$\alpha = \frac{1}{X_0}\frac{\Delta X}{\Delta T} \tag{19}$$

therefore, the value of the parameter X can be calculated at any temperature T(°C) by using

$$X = X_0\left[1 + \alpha\left(T - 20\right)\right]. \tag{20}$$

Variation of the equivalent-circuit elements have been measured in the temperature range from -20 °C to 120 °C. A first-order linear approximation can be expressed as

$$R_{\mathrm{ds}} = R_{\mathrm{ds0}}\left[1 + \alpha_R\left(T - 20\right)\right] \tag{21}$$

$$C = C_0\left[1 + \alpha_C\left(T - 20\right)\right] \tag{22}$$

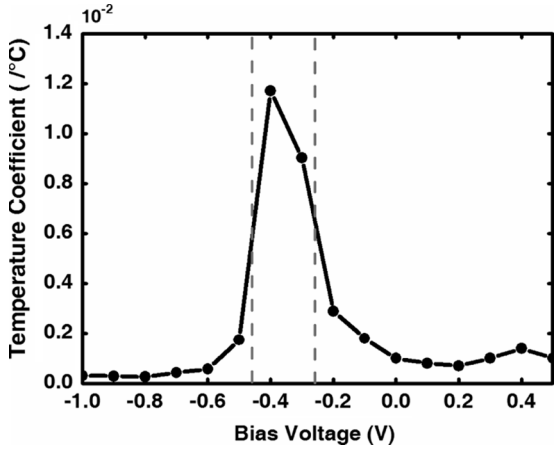

Fig. 9. Absolute values of the cold-pHEMT temperature coefficient at different biases ($f = 40$ GHz $T = 20$ °C).

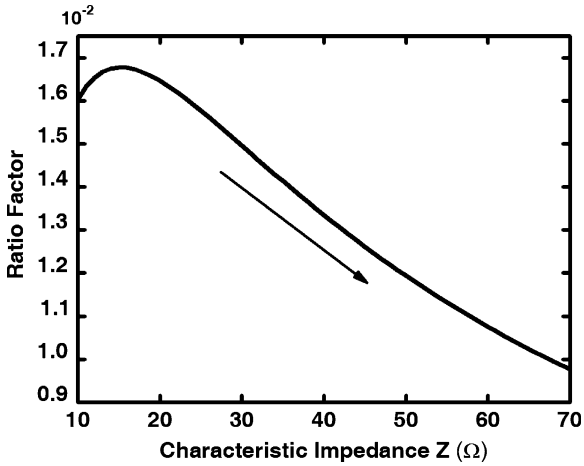

Fig. 10. Effect of Lange coupler impedance on common ratio factor.

where $R_{\rm ds0}$ and C_0 are the values measured at temperature 20 °C , and α_R and α_C are the temperature coefficients. From these equations, the temperature coefficient α_{Z_T} of the cold-pHEMT termination can be derived and written as

$$\begin{aligned}\alpha_{Z_T} &= \frac{dZ_T}{dT} \\ &= \frac{\partial Z_T}{\partial R_{\rm ds}}\frac{dR_{\rm ds}}{dT} + \frac{\partial Z_T}{\partial C}\frac{dC}{dT} \\ &= \frac{\alpha_R R_{\rm ds0}}{(1+j\omega R_{\rm ds0}C_0)^2} - \frac{j\alpha_C \omega C_0 R_{\rm ds0}^2}{(1+j\omega R_{\rm ds0}C_0)^2}. \end{aligned} \quad (23)$$

Fig. 9 illustrates the absolute value of (23) at different bias voltages. When the bias is set between -0.45 and -0.25 V, the temperature coefficient increases notably. Therefore, practical applications should avoid using the cold-pHEMT working in this region for its excessive temperature fluctuation.

Based on the analysis of the cold-pHEMT, the temperature drift of the bi-phase amplitude modulator can be approximately estimated. For the unbalanced and balanced bi-phase amplitude modulators, the temperature coefficient α_U and α_B are given by

$$\alpha_U = \frac{dS_{21}}{dT} = \frac{-2j\alpha_{Z_T}Z}{(Z_{T0}+Z)^2} \quad (24)$$

$$\alpha_B = \frac{dS_{21}}{dT} = \frac{j\alpha_{Z_{T1}}Z}{(Z_{T1}+Z)^2} - \frac{j\alpha_{Z_{T2}}Z}{(Z_{T2}+Z)^2}. \quad (25)$$

From these equations, the mathematical method can further deduce that the balanced topology has better temperature performance than the unbalanced topology. In both α_U and α_B, there is a common ratio factor M given by

$$M = \frac{Z}{(Z_T+Z)^2} \quad (26)$$

which demonstrates the temperature performance is dependent on the Lange coupler characteristic impedance. Fig. 10 illustrates the effect of Lange coupler impedance Z on the temperature drift with a specific Z_T. Obviously, as it shows, the temperature drift can approximately be regarded as a descending function of Z. Therefore, in order to obtain better temperature performance, the higher impedance Lange coupler should be used, and this conflicts with the proposed method to get high modulating performance.

IV. Circuit Design and Measurement Results

The key point in circuit design is to determine the parameters of cold-pHEMT terminations and Lange couplers. From the preceding analysis, there are not the most optimum parameters for the vector modulator to get both the highest performance and the lowest temperature drift. Therefore, there should be a compromise between the two goals. For the unbalanced vector modulator, 40 Ω is ultimately selected to be the characteristic impedance value of Lange coupler, and from the contour shown in Fig. 5, the optimum total gatewidth of the cold-pHEMT is 90 μm (2 × 45 μm). In the same way, 40 Ω is also selected to be the impedance value of Lange coupler for the balanced vector modulator, and the optimum total gatewidth of the cold-pHEMT is 130 μm (2 × 65 μm).

A great deal of research has been done on synthesis of the Lange coupler with the given parameters. To design a Lange coupler with the characteristic impedance less than 50 Ω, linewidth w increases and line gap s decreases. Using the approximate computing procedure [10], a 3-dB Lange coupler with 40-Ω characteristic impedance requires $w = 12$ μm and $s = 7.5$ μm. The total length of the Lange coupler will be around 700 μm considering interconnect structures in the layout process.

Based on the selected parameters, two 40-GHz vector modulator MMICs of different type topologies were fabricated on a 100-μm-thick GaAs substrate with 0.15-μm pHEMT devices. The microphotographs of these two circuits are shown in Fig. 11. The unbalanced vector modulator has a chip size of 1.9 mm × 0.7 mm, and the balanced vector modulator has a chip size of 1.9 mm × 1.5 mm. Though the unbalanced vector modulator has four bias pads, each two adjacent pads are using one control signal in common.

A. Static Performance

The frequency response and static constellation were measured using a Cascade on-wafer probe station and HP8722D vector network analyzer. Both vector modulators achieve good

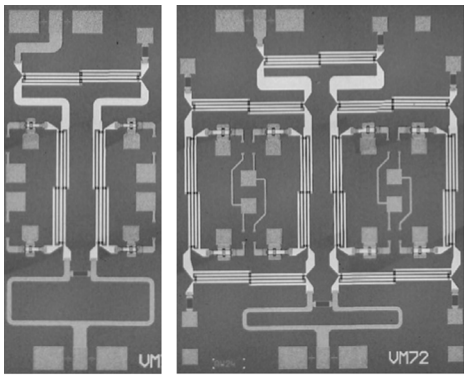

(a) (b)

Fig. 11. Microphotographs of the: (a) unbalanced vector modulator and (b) balanced vector modulator.

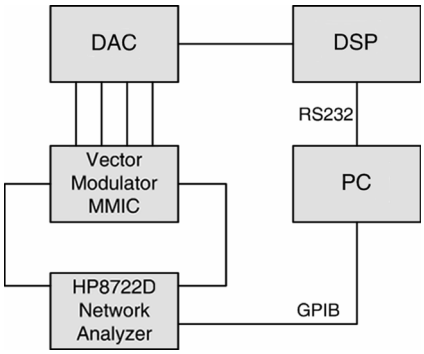

Fig. 12. Block diagram of the measurement setup.

impedance matching over 20–40 GHz. In order to obtain the static constellation automatically, a digital signal processor (DSP) controlled circuit with a digital-to-analog converter (DAC) is used in the automatic measurement system shown in Fig. 12. The DSP controlled circuit can generate four independent bias voltages sweeping from -1 to 0.5 V, in a minimum step of 10 mV. Fig. 13 shows the simulated and measured static constellations of the unbalanced vector modulator. Due to the parasitical elements of the cold-pHEMT, this constellation is skew. On the contrary, the constellations of the balanced vector modulator shown in Fig. 14 are more symmetrical owing to the push–pull topology. For both the unbalanced and balanced, the inaccuracies in modeling the cold-pHEMT and Lange coupler cause the deviation between simulation and measurement results. Compared with the reported direct carrier vector modulators MMICs, the performances are summarized in Table I.

Although there are no vector modulators operating at the same frequency to be compared with directly, the technique presented in this paper shows superiority without involving complex design process and higher cost.

B. Temperature Behavior and Drift

To obtain the temperature behavior of the vector modulators, measurements under -55 °C, -20 °C, 0 °C, 20 °C, and 70 °C have been carried out. Both two-vector modulators performed regularly under these conditions.

The amplitude drift α_{IL} and phase drift α_θ are calculated by

$$\alpha_{\mathrm{IL}} = \frac{\mathrm{IL}_{T_2} - \mathrm{IL}_{T_1}}{T_2 - T_1} \tag{27}$$

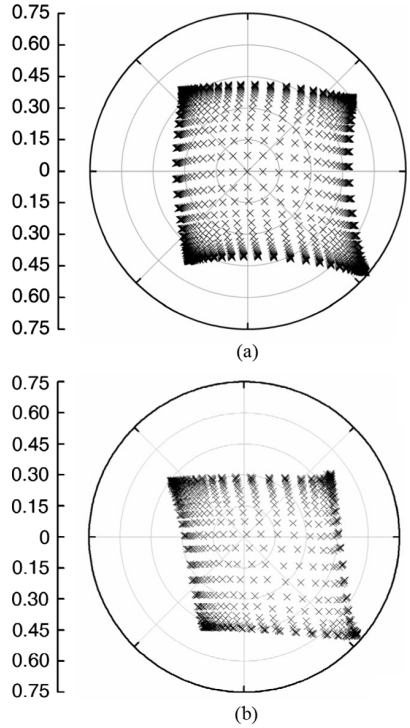

(a) (b)

Fig. 13. Static constellations of the unbalanced vector modulator. (a) Simulated and (b) measured ($f = 40$ GHz $T = 20$ °C).

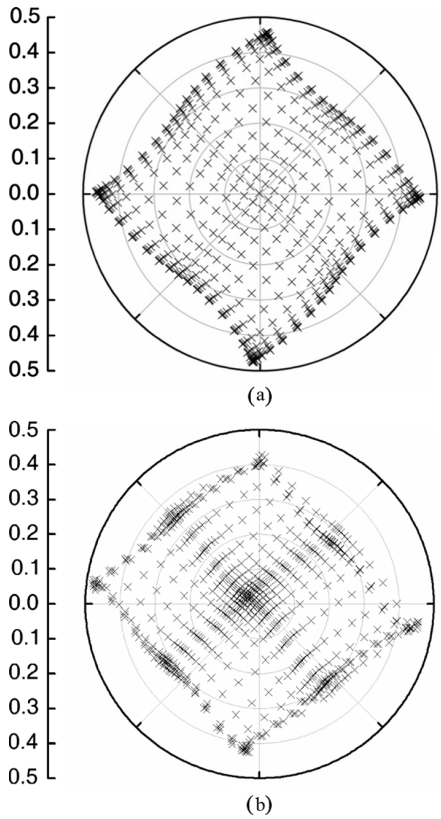

(a) (b)

Fig. 14. Static constellations of the balanced vector modulator. (a) Simulated and (b) measured ($f = 40$ GHz $T = 20$ °C).

$$\alpha_\theta = \frac{\theta_{T_2} - \theta_{T_1}}{T_2 - T_1} \tag{28}$$

TABLE I
PERFORMANCE SUMMARY OF REPORTED DIRECT CARRIER VECTOR MODULATOR MMICS

Type	Frequency Center	Performance
Balanced [11]	76.5GHz	17dB insertion loss (omnidirectional) 12dB insertion loss (minimum)
Balanced [4]	38GHz and 60GHz	11dB insertion loss ±2° phase error ±0.3dB amplitude imbalanced
Balanced [12]	110GHz	12dB insertion loss *
Balanced [13]	26GHz	13dB insertion loss (omnidirectional) 7dB insertion loss (minimum)
Unbalanced (presented in this paper)	40GHz	10.6dB insertion loss (omnidirectional)
Balanced (presented in this paper)	40GHz	10.2dB insertion loss (omnidirectional) 7.3dB insertion loss (minimum) ±1.5° phase error ±0.3dB amplitude imbalanced

* Only achieved 90° relative phase shift

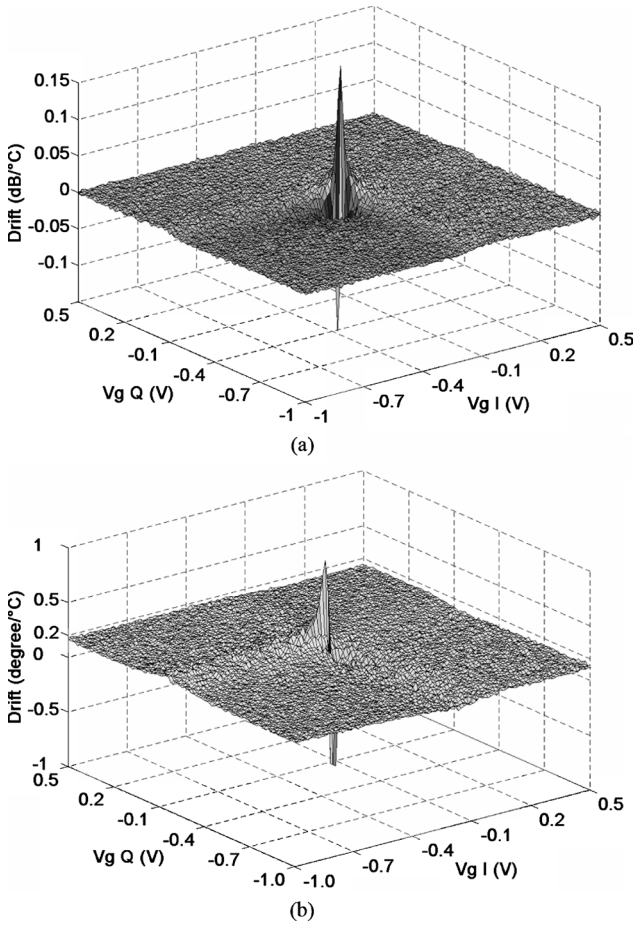

Fig. 15. Measured: (a) amplitude and (b) phase temperature drifts of the unbalanced vector modulator at 40 GHz.

where $\mathbb{L}$ and θ are the insertion loss and phase shift under different ambient temperature T. As $T_1 = -55$ °C and $T_2 = 70$ °C, the temperature drifts of the unbalanced and balanced vector modulators are shown in Figs. 15 and 16, respectively.

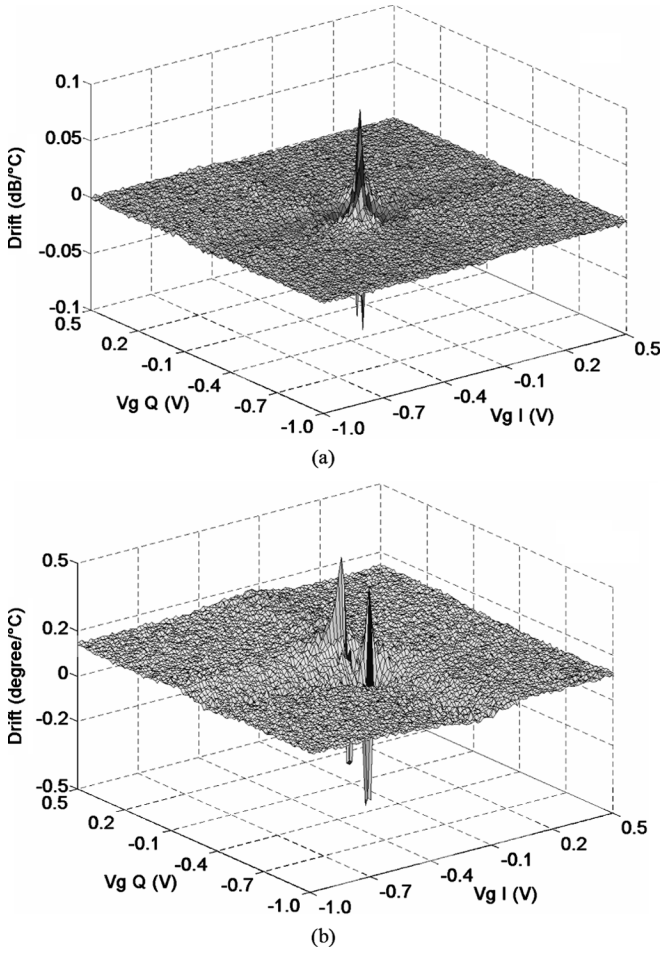

Fig. 16. Measured: (a) amplitude and (b) phase temperature drifts of the balanced vector modulator at 40 GHz.

For the unbalanced vector modulator, the typical amplitude drift and phase drift are 0.008 dB/ °C and 0.16°/ °C. The accumulative drifts between −55 °C and 70 °C are 1 dB and 20°. While for the balanced vector modulator, the typical amplitude drift and phase drift are 0.006 dB/ °C and 0.13°/ °C. The accumulative drifts between −55 °C and 70 °C are 0.75 dB and 16°. This result verifies that the balanced topology has some advantage in suppressing temperature drift. Meanwhile, from the results it can be seen that when the bias voltage is set between −0.3 and −4, the vector modulator performance is extremely sensitive to the temperature, which is also previously deduced. These data prove that the two vector modulators have good temperature performance, and the drift values can be used to do calibration when necessary.

V. CONCLUSION

An efficient technique, adjusting the cold-pHEMT total gatewidth and the Lange coupler characteristic impedance to improve the modulating performance of vector modulators, has been discussed in this paper. The thermal behavior of the vector modulator has also been taken into account. Two vector modulator MMICs employing unbalanced and balanced bi-phase amplitude modulators, respectively, were fabricated and tested. By demonstrating at 40 GHz, both vector modulators are qualified for direct carrier multilevel digital modulation in a critical temperature range between −55 °C and 70 °C.

Compared with designs published, both the minimum insertion loss of this design and the imperfection in the constellation are reduced without notably deteriorating other qualities. This design technique promises high-performance circuits with low-temperature drift and can be suitable for use up to the submillimeter-wave band.

ACKNOWLEDGMENT

The authors would particularly like to acknowledge the contributions made by former Chinese Academy of Science, Shanghai, China, colleagues Dr. J. Gu and W. Tian.

The authors would also like to thank H. Guo, University of Strathclyde, Glasgow, U.K., for many useful discussions.

REFERENCES

[1] S. Lucyszyn, T. Sewell, and I. D. Robertson, "Multi-level digital modulation performed directly at carrier frequency," in *25th Eur. Microw. Conf.*, Bologna, Italy, Sep. 1995, pp. 673–676.

[2] V. Cannistraro, J. C. Liou, and S. McCarter, "Direct modulation lowers VSAT equipment costs," *Microw. RF*, pp. 99–101, Aug. 1990.

[3] L. M. Devlin and B. J. Minnis, "A versatile vector modulator design for MMIC," in *IEEE MTT-S Int. Microw. Symp. Dig.*, May 1990, pp. 519–521.

[4] A. E. Ashtiani, S.-I. Nam, A. d'Espona, S. Lucyszyn, and I. D. Robertson, "Direct multilevel carrier modulation using millimeter-wave balanced vector modulators," *IEEE Trans. Microw. Theory Tech.*, vol. 46, no. 12, pp. 2611–2619, Dec. 1998.

[5] S. Nam, N. Shala, K. S. Ang, A. E. Ashtiani, I. D. Robertson, and S. P. Marsh, "Monolithic millimeter-wave balanced bi-phase amplitude modulator in GaAs/InGap HBT technology," in *IEEE MTT-S Int. Microw. Symp. Dig.*, Anaheim, CA, Jun. 1999, pp. 243–246.

[6] M. Chongcheawchamnan, S. Bunnjaweht, D. Kpogla, D. Lee, and I. D. Robertson, "Microwave I-Q vector modulator using a simple technique for compensation of FET parasitics," *IEEE Trans. Microw. Theory Tech.*, vol. 50, no. 6, pp. 1642–1646, Jun. 2002.

[7] Y. Hou, X. Sun, and L. Li, "An efficient technique for designing balanced vector modulators with low insertion loss," in *IEEE MTT-S Int. Microw. Symp. Dig.*, Atlanta, GA, Jun. 15–20, 2008, pp. 1281–1284.

[8] S. Marsh, *Practical MMIC Design*. Norwood, MA: Artech House, 2006, pp. 231–245.

[9] R. E. Anholt and S. E. Swirhun, "Experimental investigation of the temperature dependence of GaAs FET equivalent circuits," *IEEE Trans. Electron Devices*, vol. 39, no. 9, pp. 2029–2036, Sep. 1992.

[10] D. Kajfez, Z. Paunovic, and S. Pavlin, "Simplified design of Lange coupler," *IEEE Trans. Microw. Theory Tech.*, vol. MTT-26, no. 10, pp. 806–808, Oct. 1978.

[11] D. S. McPherson and S. Lucyszyn, "Vector modulator for W-band software radar techniques," *IEEE Trans. Microw. Theory Tech.*, vol. 49, no. 8, pp. 1451–1461, Aug. 2001.

[12] D. S. McPherson, H. Seo, Y. Jing, and S. Lucyszyn, "110 GHz vector modulator for adaptive software-controlled transmitters," *IEEE Trans. Microw. Theory Tech.*, vol. 11, no. 1, pp. 16–18, Jan. 2001.

[13] C. Y. Ng, M. Chongcheawchamnan, and I. D. Robertson, "A balanced vector modulator for LMDS applications," in *IEEE High Freq. Postgraduate Student Colloq.*, Sep. 2001, pp. 152–157.

Yang Hou (S'08) was born in Shenyang, China, in 1983. He received the B.S. degree in electrical and electronic engineering from the University of Science and Technology of China, Hefei, China, in 2005, and is currently working towards the Ph.D. degree in RF and microwave microelectronics at the Chinese Academy of Sciences, Shanghai, China.

He is currently with the Shanghai Institute of Microsystem and Information Technology, Chinese Academy of Sciences, Shanghai, China. His current research interests are RF integrated circuits design and MMIC designs of transceivers for millimeter-wave communication applications.

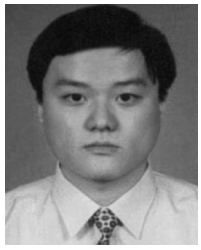

Lingyun Li received the B.S. degree in communication engineering and Ph.D. degree in electrical engineering from Shanghai JiaoTong University, Shanghai, China, in 2000 and 2005, respectively.

He is currently with the Shanghai Institute of Microsystem and Information Technology, Chinese Academy of Sciences, Shanghai, China. His current research interests are in the areas of MMIC design, RF CMOS integrated circuits modeling and design, high-frequency measurement technology, and radio remote-sensor systems.

Rong Qian was born in Shanghai, China, in 1968. She is currently with the Shanghai Institute of Microsystem and Information Technology, Chinese Academy of Sciences, Shanghai, China.

Her current research interests are in millimeter-wave electron devices and measurement techniques.

Xiaowei Sun (M'00) was born in Beijing, China, in 1958. She received the B.S. degree in electronics from Xian Jiaotong University, Xian, China, in 1982, the M.S. degree in electronics from the Graduate University of Chinese Academy of Sciences, Beijing, China, in 1984, and the Ph.D. degree in microelectronics from Xian Jiaotong University, Xian, China, in 1996.

She was an Associate Professor with Xidian University for ten years. Since 1997, she joined the Shanghai Institute of Microsystem and Information Technology, Chinese Academy of Sciences. She has been a Professor and Director with the Laboratory of RF and Energy Microsystem Technology. From 1999 to 2000, she was a Visiting Professor with Sheffield University, Sheffield, U.K. She is an Adjunct Professor with Shanghai Jiaotong University, Shanghai, China. She has authored or coauthored over 80 papers in journals and academic conferences. She holds approximately 20 patents. Her research interests have been in the fields of RF and MMIC chips design\MMIC process\testing methods on probe stations, and also millimeter-wave devices and subsystems.